Available online at www.sciencedirect.com
ScienceDirect
Journal of Catalysis 252 (2007) 39–48
JOURNAL OF CATALYSIS
www.elsevier.com/locate/jcat

Promoting mechanism of potassium in preferential CO oxidation on Pt/Al_2O_3

Masatoshi Kuriyama [a], Hisanori Tanaka [a], Shin-ichi Ito [a], Takeshi Kubota [b], Toshihiro Miyao [c], Shuichi Naito [c], Keiichi Tomishige [a,*], Kimio Kunimori [a,*]

[a] *Institute of Materials Science, University of Tsukuba, 1-1-1 Tennodai, Tsukuba, Ibaraki 305-8573, Japan*
[b] *Department of Material Science, Shimane University, Matsue 690-8504, Japan*
[c] *Department of Applied Chemistry, Faculty of Engineering, Kanagawa University, 3-27-1 Rokkakubashi, Kanagawa-ku, Yokohama, Kanagawa 221-8686, Japan*

Received 5 May 2007; revised 5 July 2007; accepted 4 September 2007

Available online 29 September 2007

Abstract

The addition of potassium enhanced the activity of preferential CO oxidation on Pt/Al_2O_3. The additive effect of potassium weakened the interaction between CO and Pt, and also changed the CO adsorption site. FTIR observations under the PROX conditions suggested the presence of adsorbed species derived from O_2 and H_2 such as OH species, which can be related to the promoting effect of H_2 present in the PROX reaction.

Keywords: Preferential CO oxidation; Platinum; Al_2O_3; Potassium

1. Introduction

Hydrogen is a promising energy carrier associated with fuel cell technology [1], where one hydrogen production method is the steam-reforming reaction of hydrocarbons and oxygenates. In this case, the product of gases can contain CO as an impurity, which can be considered a poison for the anode catalyst [2–4]. Preferential CO oxidation in H_2-rich mixtures is an important reaction in terms of the purification of fuel gas [5].

There have been many reports on supported noble metal catalysts, such as Pt [6–33], Pd [15,34], Ru [15,35] and Rh [36–39], for preferential CO oxidation in H_2-rich gas. In particular, the effect of various additives has been investigated [6,11,18,19,24,25,27]. In addition, Au [40–46] and Cu [47–50] catalysts also exhibit high performance, which generally can be explained by the weaker interaction with CO compared with noble metal catalysts. Recently, the addition of alkali metal to noble metal catalysts in preferential CO oxidation has been reported [6–8,34,36–39]. Pt clusters supported on Cs-modified SiO_2 showed higher turnover rate and selectivity than clusters of similar size dispersed on SiO_2 and Al_2O_3; the modification effect can be explained by the disruption of CO monolayer growth through promotion of the formation of unreactive chemisorbed carbon via CO dissociations and disproportionation [6]. In contrast, in the case of Pt/Al_2O_3 modified with potassium, the adsorption site of CO on Pt was changed drastically, and the interaction between CO and Pt became weaker with the addition of potassium [51]. Our group has reported that the optimized $K–Pt/Al_2O_3$ catalyst was very effective in decreasing CO concentration to <10 ppm in fuel gas; in particular, the activity of CO oxidation was promoted drastically by the presence of H_2 [7,8]. In the present work, we investigated the effect of potassium on catalytic properties in preferential CO oxidation by means of transmission electron microscopy (TEM), extended X-ray adsorption fine structure (EXAFS), X-ray near-edge structure (XANES), and in situ Fourier transform infrared spectroscopy (FTIR). In particular, we attempted to elucidate the promoting mechanism of potassium on Pt/Al_2O_3 in preferential CO oxidation.

* Corresponding authors. Faxes: +81 29 853 4490; +81 29 853 5030.
E-mail addresses: tomi@tulip.sannet.ne.jp (K. Tomishige), kunimori@ims.tsukuba.ac.jp (K. Kunimori).

0021-9517/$ – see front matter
doi:10.1016/j.jcat.2007.09.001

2. Experimental

2.1. Catalyst preparation

The Al_2O_3 support (JRC-ALO-4 from Japan Reference Catalyst [JRC]; BET surface area, 170 m^2/g) was used as support materials. Before impregnation, Al_2O_3 was calcined for 3 h in air at 873 K. Pt/Al_2O_3 catalyst was prepared by impregnating the Al_2O_3 with an aqueous solution of $Pt(NO_2)_2(NH_3)_2$ (Soekawa Chemical Co., Ltd.). After impregnation, the sample was dried at 383 K for 12 h and then calcined in air at 773, 823, and 873 K for 3 h. The calcination temperature of the catalysts is denoted in an angle bracket, for example, Pt/Al_2O_3 [773]. The loading amount of Pt was 2 wt%. The Pt/Al_2O_3 catalysts modified with potassium also were prepared, and the modification method was as follows. After the impregnation with the aqueous solution of $Pt(NO_2)_2(NH_3)_2$, the sample was dried at 383 K for 12 h. After further impregnation of the dried sample with an aqueous solution of KNO_3 (Wako Pure Chemical Industries, Ltd.), it was dried again at 383 K for 12 h and calcined at 773 K for 3 h. The loading amount of potassium is described in the molar ratio to Pt (K/Pt = 10). The Pt/Al_2O_3 catalysts modified with potassium are denoted as K–Pt/Al_2O_3 and the molar ratio of K/Pt is shown in parentheses like K–Pt/Al_2O_3 (10). The catalysts were reduced with hydrogen at 773 K for 1 h in the reactor before the activity test.

2.2. Activity test of preferential CO oxidation and related reactions

Preferential CO oxidation in H_2-rich gas was carried out in a fixed-bed flow reaction system at atmospheric pressure using 100 mg of the catalyst at the total flow rate of 100 cm^3/min (STP) (GHSV = 30,000 h^{-1}). The feed stream contained 0.2% CO, 0.2% O_2, and 75% H_2, and it was balanced with helium. The effluent gas was analyzed using an online gas chromatograph (GC) system equipped with a thermal conductivity detector. The activity was evaluated by CO and O_2 conversions, which can be calculated on the basis of CO and O_2 concentrations in the reactant gas and the effluent gas. The selectivity of CO oxidation is defined as the ratio of O_2 consumption for the CO oxidation to the total O_2 consumption. The preferential CO oxidation in H_2-rich stream is denoted as PROX here. As a reference, we also carried out the activity test of CO oxidation in the absence of H_2. Here the feed stream contained 0.2% CO, 0.2% O_2, and it was balanced with helium. This CO oxidation in the absence of H_2 is denoted as CO + O_2. As another reference, the activity of the water–gas shift reaction was also tested; the feed contained 0.2% CO, 3% H_2O, and balance He. The steam is introduced by a gas-stripping method. In all reactions, the activity was observed for 30 min at each condition. Because almost no deactivation was observed, the results of the activity test correspond to those under the steady-state condition.

2.3. Catalyst characterization

2.3.1. Measurement of adsorption amount of CO and H_2

The catalysts were characterized by the amounts of H_2 and CO adsorption. The amount of the irreversible adsorption of H_2 and CO (H/Pt, CO/Pt) was measured at room temperature in a vacuum system (sample weight, 0.15 g; dead volume, 65 cm^3) by the volumetric method [38]. The samples are pretreated in O_2 at 773 K for 1 h, followed by H_2 reduction at 773 K for 1 h at atmospheric pressure. The equilibrium pressure of H_2 and CO was about 1.0 kPa.

2.3.2. TEM observation

Transmission electron microscope (TEM) images were obtained using a JEOL JEM-2010F microscope operated at 200 kV. First, the catalysts were reduced by H_2 pretreatment at 773 K for 1 h in a fixed-bed reactor. After the reduction, samples were stored under vacuum until the measurements were made. Samples were dispersed in 2-propanol using supersonic waves, and they were put on Cu grids for TEM observation under air atmosphere. Average particle size (d) is calculated by $d = \sum n_i d_i^3 / \sum n_i d_i^2$ (n_i, number of pieces; d_i, particle size) [52].

2.3.3. EXAFS and XANES

Pt L_3-edge EXAFS and XANES spectra was measured at the BL-12C station of the Photon Factory at the High-Energy Accelerator Research Organization (proposal 2005G041). The storage ring was operated at 2.5 GeV. A Si(111) single crystal was used to obtain a monochromatic X-ray beam. The monochromator was detuned to 60% maximum intensity to avoid higher harmonics in the X-ray beam. Two ion chambers filled with Ar and 15% Ar diluted N_2 for Pt L_3-edge EXAFS were used as detectors of I and I_0, respectively. The samples for the measurement were prepared by pressing 200 mg of catalyst powder to disks. The thickness of the samples was chosen as 0.6–0.7 mm (10 mm φ), to give an edge jump of 0.7. The samples were pretreated at 773 K with H_2 for 1 h. After the pretreatment, we transferred the samples to the measurement cell without exposing the sample disk to air, using a glove box filled with nitrogen. EXAFS and XANES data were collected in transmission mode at room temperature. For EXAFS analysis, the oscillation was first extracted from the EXAFS data by a spline smoothing method [53]. The oscillation was normalized by the edge height at ca. 50 eV. The Fourier transformation of the k^3-weighted EXAFS oscillation from k space to r space was performed over the range of 30–160 nm^{-1} to obtain a radial distribution function. The inversely Fourier filtered data were analyzed by a common curve-fitting method [54,55]. For the curve-fitting analysis, the empirical phase shift and amplitude functions for Pt–Pt and Pt–O bonds were extracted from the data for Pt foil and $Na_2Pt(OH)_6$, respectively. In the analysis of XANES spectra, the normalized spectra were obtained by subtracting the pre-edge background from the raw data with a modified Victoreen equation and normalizing them by the edge height [56–59]. The EXAFS data were analyzed using REX2000 version 2.3.3 (Rigaku Corp.).

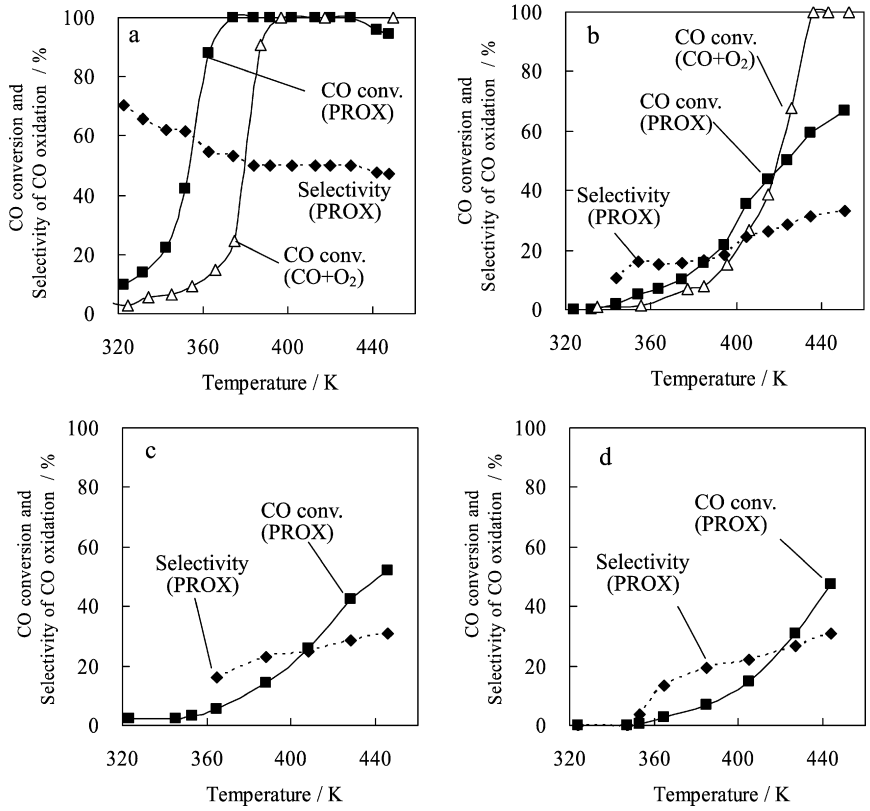

Fig. 1. Reaction temperature dependence of CO conversion (■, △) and selectivity of CO oxidation (◆) in PROX and CO + O_2 reactions. (a) K–Pt/Al_2O_3 (10), (b) Pt/Al_2O_3 [773], (c) Pt/Al_2O_3 [823], (d) Pt/Al_2O_3 [873] Reaction conditions: PROX: 0.2% CO, 0.2% O_2, 75% H_2, He balance (■, ◆); CO + O_2: 0.2% CO, 0.2% O_2, He balance (△).

2.3.4. FTIR measurements

FTIR spectra were recorded with a Nicolet Magna 550 spectrometer equipped with a MCT detector (resolution, 4 cm^{-1}) in a transmission mode, using an in situ IR quartz cell with CaF_2 windows. All samples for the IR measurements were pressed into self-supporting 20-mm-diameter, 300-mg wafers. The sample was transferred to the IR cell connected to the closed circulation systems and then reduced with H_2 at 773 K for 1 h at 13 kPa. After pretreatment, the sample was cooled to 313 K, and the gases (CO, CO + O_2, CO + O_2 + H_2) were introduced to the IR cell connected to the flow and evacuating system. Temperature dependence of the FTIR spectra during the reactions was measured for 15 min at each temperature. The FTIR spectra of adsorbed species were obtained by subtracting the spectra before the reaction at the same temperature. The total gas flowing rate in all of the reactions was adjusted to GHSV = 30,000 h^{-1}, which was used for the activity tests in the fixed-bed reactor.

3. Results and discussion

3.1. Catalytic performance in PROX and CO + O_2

Fig. 1 shows the effects of reaction temperature on the performance of the PROX and CO + O_2 reactions. K–Pt/Al_2O_3 (10) showed much higher activity and selectivity than all of the Pt/Al_2O_3 catalysts in the PROX reaction [7,8]. The CO conversion in the PROX on K–Pt/Al_2O_3 (10) reached almost 100% in the temperature range of 383–430 K. This behavior is useful, because it avoids the need for careful temperature control. In particular, according our previous report, K–Pt/Al_2O_3 (10) gave CO concentrations <10 ppm as a result of the PROX reaction in the temperature range of 375–410 K [7]. As shown in Fig. 1a, CO conversion was much higher in the PROX reaction than in the CO + O_2 reaction, suggesting that the presence of H_2 significantly promotes CO oxidation on K–Pt/Al_2O_3 (10). In contrast, as shown in Fig. 1b, CO conversion in the PROX reaction on Pt/Al_2O_3 [773] was lower than that in the CO + O_2 reaction at the reaction temperatures above 420 K. This can be related to the low selectivity of CO oxidation in PROX on Pt/Al_2O_3 [773]. The amounts of CO and H_2 adsorption on K–Pt/Al_2O_3 (10) and three Pt/Al_2O_3 catalysts are given in Table 1. The adsorption of the Pt/Al_2O_3 catalysts decreased gradually with increasing calcination temperature due to aggregation of Pt metal particles. Note that the CO adsorption of K–Pt/Al_2O_3 (10) was comparable to that of Pt/Al_2O_3 [823]. Based on the result of CO adsorption, it is possible to estimate the turnover frequency (TOF) of CO oxidation, as also given in Table 1. Regarding the Pt/Al_2O_3 catalysts, the TOF in PROX increased slightly with decreasing adsorption and metal dispersion. This tendency agrees with previously reported findings [33]. It has been reported that flat surfaces have a significantly higher CO oxidation activity per surface site compared with low-coordination edge and corner atoms in the PROX reaction [33]. In addition, it is characteristic that K–Pt/Al_2O_3 (10) gave much higher TOF of CO oxidation

Table 1
Adsorption amount of H_2, CO and TOF of CO_2 formation over K–Pt/Al_2O_3 and Pt/Al_2O_3 catalysts at 363 K

Catalyst	Calcination temperature (K)	Adsorption amount		TOF ($\times 10^{-3}$ s^{-1})[a]		
		H/Pt[b]	CO/Pt[b]	$CO + O_2$[c]	$CO + O_2 + H_2$[d]	$CO + H_2O$[e]
K–Pt/Al_2O_3 (10)	773	0.38	0.40	5.4	32[f]	1.3
Pt/Al_2O_3 [773]	773	0.70	0.52	1.0	1.9	0.03
Pt/Al_2O_3 [823]	823	0.53	0.37	–	2.2	–
Pt/Al_2O_3 [873]	873	0.14	0.14	–	2.6	–

[a] TOF of CO oxidation is calculated on the basis of CO/Pt.
[b] Irreversible adsorption of H_2 and CO at room temperature.
[c] 0.2% CO, 0.2% O_2, He balance.
[d] 0.2% CO, 0.2% O_2, 75% H_2, He balance.
[e] 0.2% CO, 3% H_2O, He balance.
[f] The TOF was calculated by an extrapolating method in the Arrhenius plot at the temperature range of 323–353 K because K–Pt/Al_2O_3 (10) gave 88% CO conversion at 363 K.

in PROX than the Pt/Al_2O_3 catalysts. Furthermore, the TOF in PROX was much higher than that in $CO + O_2$ on K–Pt/Al_2O_3 (10). One of the promoting mechanisms of H_2 to CO oxidation may be due to the water–gas shift reaction originating from H_2 oxidation to H_2O on the basis of previous reports [9,23–27]. Therefore, the activity of the water–gas shift reaction was also measured; the TOFs obtained are given in Table 1. The TOFs of the water–gas shift reaction were much lower than those in the PROX and $CO + O_2$ reactions, and the promotion of H_2 to CO oxidation cannot be explained by the water–gas shift reaction in the present case.

3.2. Catalyst characterization by TEM, EXAFS, and XANES

Fig. 2 shows TEM images of the Pt/Al_2O_3 [773] and K–Pt/Al_2O_3 (10) catalysts. The average particle sizes of Pt/Al_2O_3 [773] and K–Pt/Al_2O_3 (10) were determined to be 0.5 ± 0.1 and 2.0 ± 0.3 nm, respectively. The tendency for K–Pt/Al_2O_3 (10) to have lower dispersion than Pt/Al_2O_3 [773] agrees well with the results on adsorption (Table 1).

Fig. 3 shows the result of Pt L_3-edge EXAFS analysis of these catalysts, and Table 2 gives curve-fitting results. The Pt–Pt and Pt–O bonds were required for the curve fitting of Pt/Al_2O_3 [773] and [823], although the contribution of the Pt–O bond was rather small. This suggests that highly dispersed Pt metal particles interact with the surface of the Al_2O_3 support. The coordination number of the Pt–Pt bond on Pt/Al_2O_3 increased monotonously with increasing calcination temperature. We conclude that aggregation of Pt metal particles occurs by calcination at higher temperatures. The coordination number of the Pt–Pt bond on K–Pt/Al_2O_3 (10) was located between that of Pt/Al_2O_3 [773] and [823], and the tendency was similar to that of the adsorption amount of CO. This may be related to the neutralization of the acidic properties of Al_2O_3, which can contribute to the enhanced metal dispersion.

Fig. 4 shows the results of Pt L_3-egde XANES spectra, and Table 3 gives the results of the XANES analysis. The white line intensity of Pt L_3-edge is known to be an informative indication of the electronic state of Pt; the larger white line is due to the greater electron vacancy in d-orbital [60]. As reported previously, a relative electron deficiency of the Pt species can be determined based on the white line intensity [56–59].

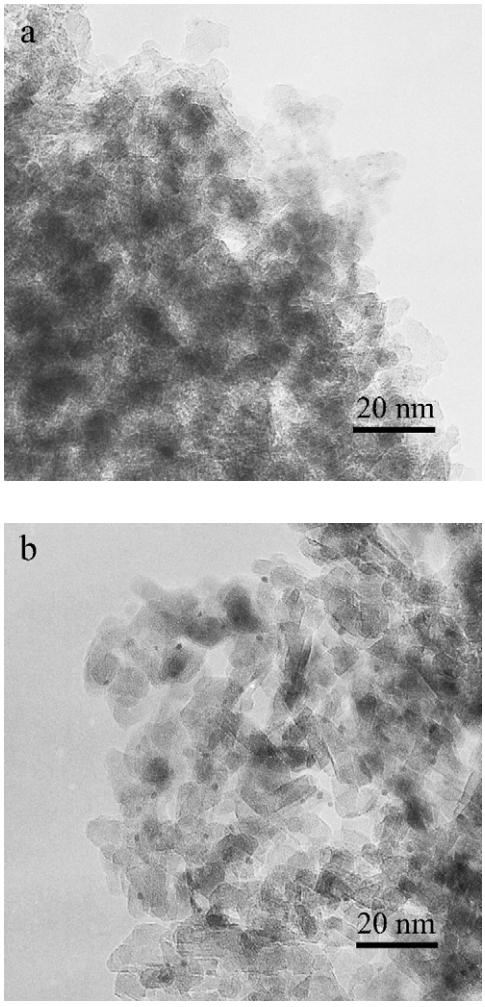

Fig. 2. TEM images of (a) fresh Pt/Al_2O_3 [773] and (b) K–Pt/Al_2O_3 (10) after H_2 reduction.

For the Pt/Al_2O_3 catalysts, the relative electron deficiency decreased gradually with increasing calcination temperature. This may be associated with the decreased contribution of the Pt–O bond in EXAFS results as well as the decreased metal dispersion. On the other hand, the relative electron deficiency of K–Pt/Al_2O_3 (10) was positioned between that of Pt/Al_2O_3 [773] and [823].

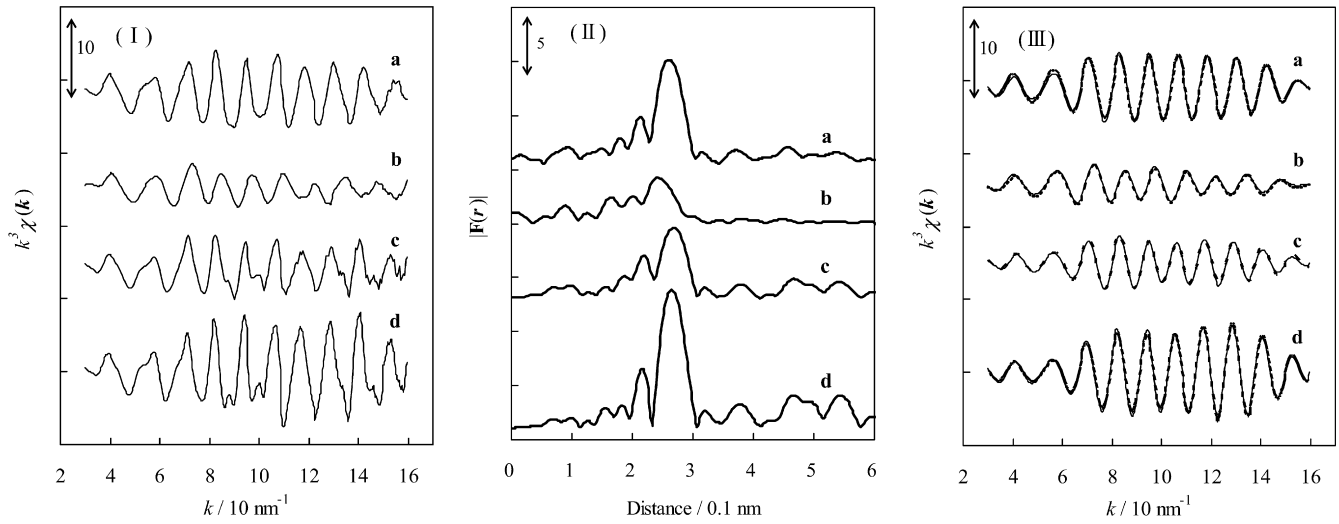

Fig. 3. Results of Pt L_3-edge EXAFS analysis of K–Pt/Al_2O_3 (10) and Pt/Al_2O_3 catalysts after the H_2 reduction. (I) k^3-weighted EXAFS oscillations. (II) Fourier transforms of k^3-weighted Pt L_3-edge EXAFS, FT range: 30–160 nm^{-1}. (III) Fourier filtered EXAFS data (—) and calculated data (- - -). Fourier filtering range: 0.16–0.31 nm: (a) K–Pt/Al_2O_3 (10), (b) Pt/Al_2O_3 [773], (c) Pt/Al_2O_3 [823], (d) Pt/Al_2O_3 [873].

Table 2
Curve fitting results of Pt L_3-edge EXAFS of K–Pt/Al_2O_3 (10) and Pt/Al_2O_3 catalysts after H_2 reduction[a]

Catalysts	Shells	C.N.[b]	R (10^{-1} nm)[c]	σ (10^{-1} nm)[d]	ΔE_0 (eV)[e]	R_f (%)[f]
Pt/Al_2O_3 [773]	Pt–Pt	5.9 ± 0.7	2.65 ± 0.007	0.094 ± 0.007	-4.7 ± 1.8	
	Pt–O	0.9 ± 0.2	2.03 ± 0.026	0.065 ± 0.044	-5.7 ± 7.1	0.94
Pt/Al_2O_3 [823]	Pt–Pt	7.6 ± 0.6	2.78 ± 0.002	0.093 ± 0.002	6.5 ± 0.5	
	Pt–O	0.6 ± 0.5	2.12 ± 0.030	0.092 ± 0.066	2.0 ± 6.9	1.0
Pt/Al_2O_3 [873]	Pt–Pt	9.5 ± 0.4	2.78 ± 0.002	0.082 ± 0.001	1.6 ± 0.6	0.66
K–Pt/Al_2O_3 (10)	Pt–Pt	8.5 ± 0.3	2.74 ± 0.003	0.080 ± 0.012	-0.2 ± 0.8	0.69

[a] Sample pretreatment: reduction (H_2, 773 K, 1 h).
[b] Coordination number.
[c] Bond distance.
[d] Debye–Waller factor.
[e] Difference in the origin of photoelectron energy between the reference and the sample.
[f] Residual factor, Fourier filtering range: 0.16–0.38 nm.

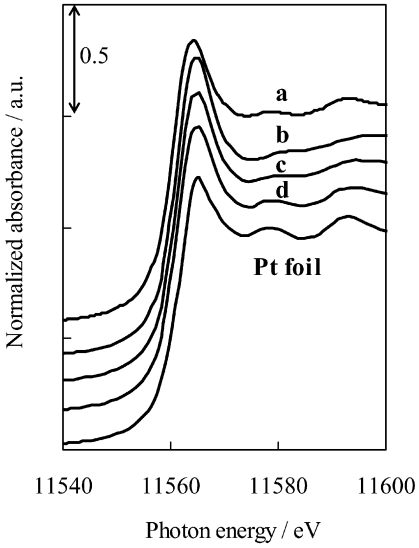

Fig. 4. Pt L_3-edge XANES spectra of K–Pt/Al_2O_3 (10) and Pt/Al_2O_3 catalysts: (a) K–Pt/Al_2O_3 (10), (b) Pt/Al_2O_3 [773], (c) Pt/Al_2O_3 [823], (d) Pt/Al_2O_3 [873].

Table 3
Results of Pt L_3-edge XANES analysis of K–Pt/Al_2O_3 (10) and Pt/Al_2O_3 catalysts

Catalysts	ΔA[a]	A[b]	$\Delta A/A$[c]
K–Pt/Al_2O_3 (10)	0.78	–	0.102
Pt/Al_2O_3 [773]	0.83	–	0.108
Pt/Al_2O_3 [823]	0.66	–	0.085
Pt/Al_2O_3 [873]	0.58	–	0.074
Pt foil	0.0	7.70	0

[a] Area difference between catalysts and Pt-foil (11540–11566 eV).
[b] White line area of Pt foil.
[c] Relative electron deficiency.

To facilitate discussion of the electronic state of the catalysts considering the Pt metal particle size, Fig. 5 shows the relationship between the coordination number of the Pt–Pt bond obtained from EXAFS and the relative electron deficiency from XANES. In the Pt/Al_2O_3 catalysts, the relative electron deficiency decreased gradually with increasing coordination number of the Pt–Pt bond. In contrast, K–Pt/Al_2O_3 (10) is far different than the relationship of the Pt/Al_2O_3 catalysts, which means

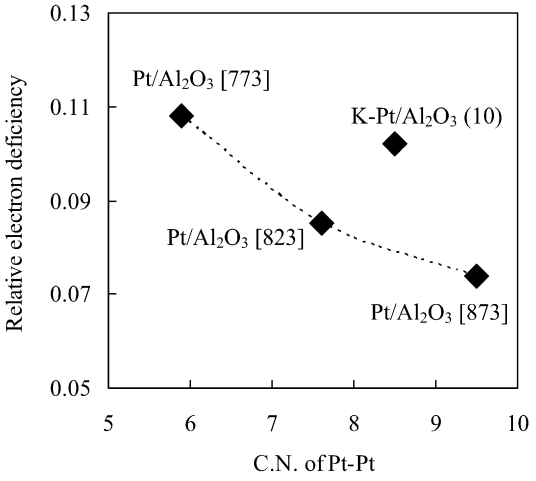

Fig. 5. Relation between the relative electron deficiency from XANES and the coordination number of the Pt–Pt bond from EXAFS of K–Pt/Al_2O_3 (10) and Pt/Al_2O_3 catalysts.

that Pt metal particles in K–Pt/Al_2O_3 (10) have a greater electron deficiency for the large Pt–Pt coordination number, possibly due to the modification of potassium. The additive effect of alkali metal to metal surfaces can be explained by electron transfer from the alkali metal to the metal surface [61–63]. This tendency is opposite to the results given earlier. The difference is due to the chemical state of alkali metal; here potassium is present as a cation, not metallic. The chemical state of the potassium was investigated by TPR with H_2. In the profile, the H_2 consumption peak due to the reduction of potassium ions to metal species was not observed, indicating that the potassium was not metallic even after H_2 reduction.

3.3. Behavior of adsorbed CO during the reaction using in situ FTIR

Fig. 6 shows the effect of evacuation temperature on IR spectra of CO adsorption over K–Pt/Al_2O_3 (10) and Pt/Al_2O_3 [773]. On K–Pt/Al_2O_3 (10), three peaks were observed. The peaks at 2059 and 1979 cm^{-1} can be assigned to linear and bridge CO on Pt, respectively [51]. Note that the peak observed at 1760 cm^{-1} was not observed on Pt/Al_2O_3; it has been suggested that this peak can be assigned to a threefold-coordinated CO species on the Pt atoms interacting with potassium species [51]. Linear, bridge, and threefold CO are denoted as L-CO, B-CO, and T-CO, respectively. The changes in the peak intensities are plotted in Fig. 6III. Almost all of the CO adsorbed on K–Pt/Al_2O_3 (10) was desorbed at 513 K; in contrast, a significant amount of CO remained on Pt/Al_2O_3 [773] even at 633 K. This indicates that the interaction of CO with K–Pt/Al_2O_3 (10) is much weaker than that with Pt/Al_2O_3 [773]. This finding agrees with previously reported results [51] and also can be related to the higher relative electron deficiency of K–Pt/Al_2O_3 (10).

Fig. 7 shows the temperature dependence of IR spectra of K–Pt/Al_2O_3 (10) during the PROX and CO + O_2 reactions and the introduction of CO. The spectrum during the introduction of CO at 313 K was almost the same as that shown in Fig. 6I, but with the difference that CO can be adsorbed even at 453 K

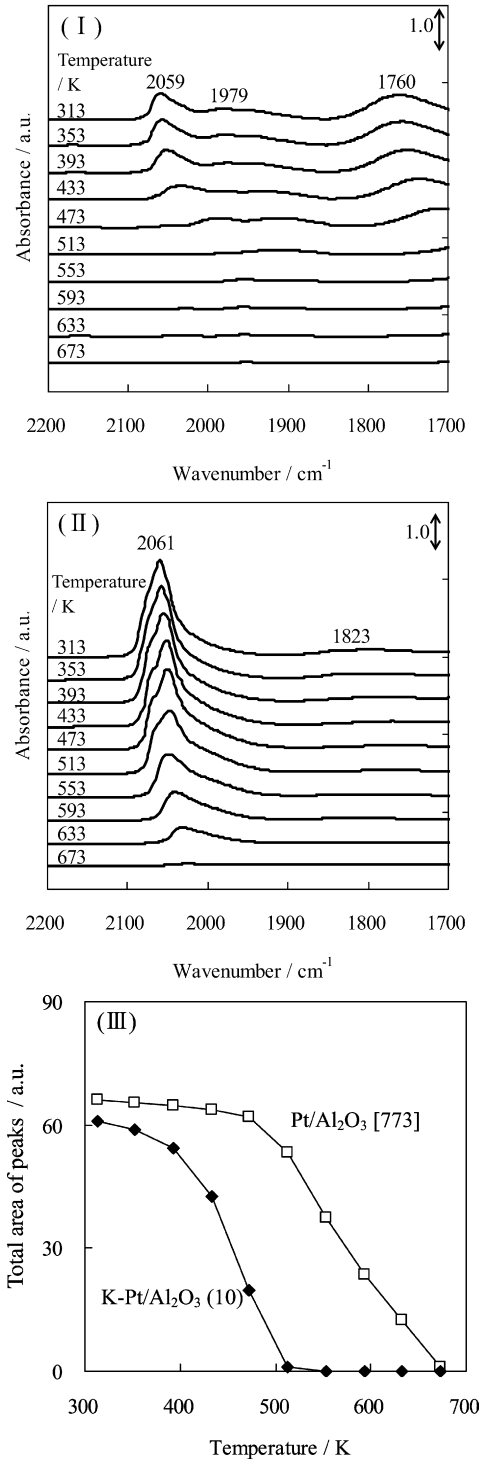

Fig. 6. Effect of evacuation temperature on IR spectra of adsorbed CO on (I) K–Pt/Al_2O_3 (10) and (II) Pt/Al_2O_3 [773] catalysts, and (III) temperature dependence of total area of the CO adsorption peaks on the catalysts. The samples were exposed to 0.3 kPa CO at 313 K and evacuated.

in the presence of gas-phase CO (Fig. 7c). The peak intensities of L-CO, B-CO, and T-CO are plotted in Fig. 7f. The order of the peak intensity in this temperature range was as follows: T-CO > B-CO > L-CO. In contrast, in the CO + O_2 reaction (Fig. 7b), the shape of the spectra differed from that for the introduction of CO. As shown in Fig. 7e, the order of the peak

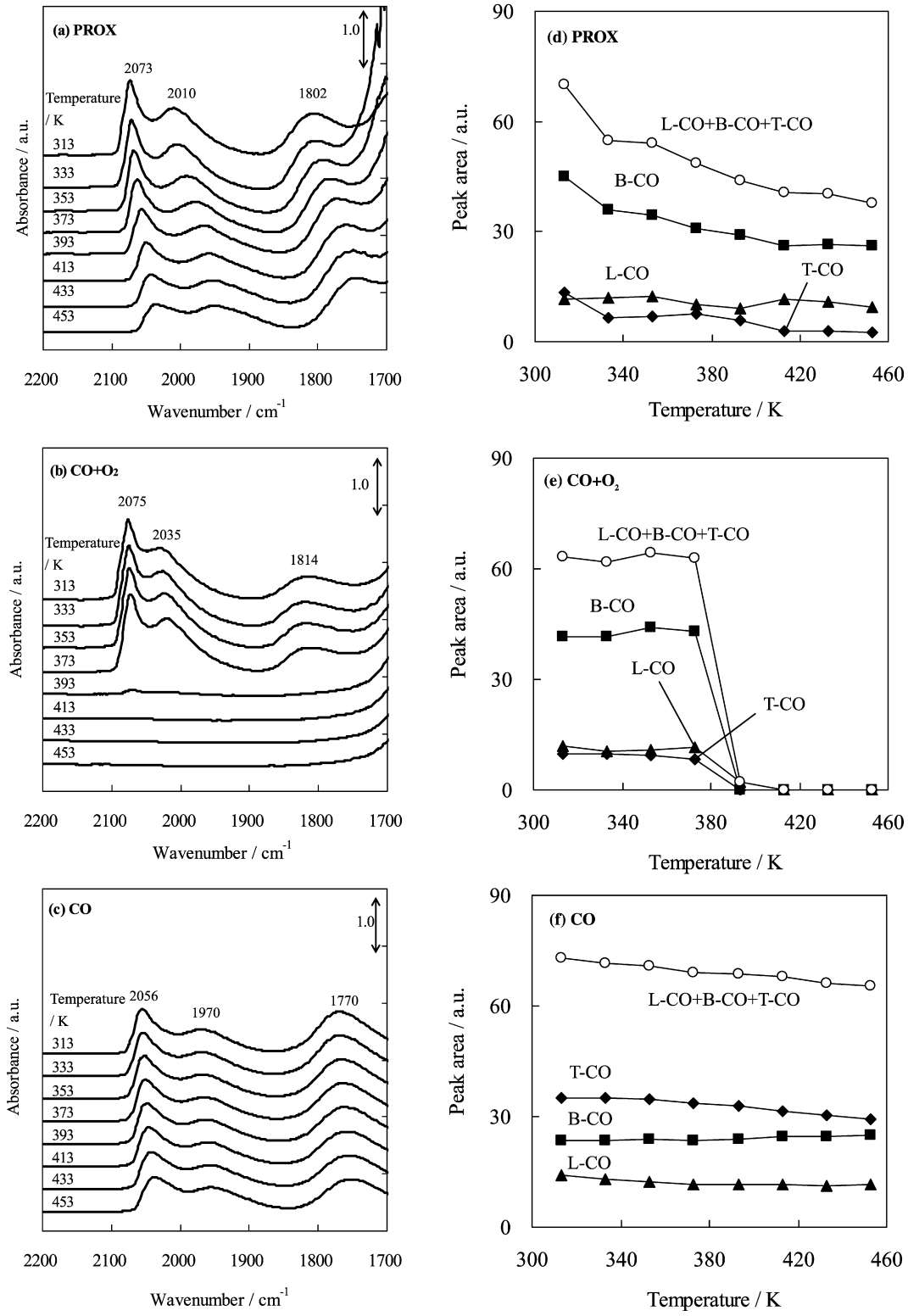

Fig. 7. Effect of temperature on IR spectra of K–Pt/Al_2O_3 (10) catalyst during PROX (a), $CO + O_2$ (b) reactions and CO (c) introduction, (d–f) area of each peak as a function of temperature. Reaction conditions: PROX: 0.2% CO, 0.2% O_2, 75% H_2, He balance; $CO + O_2$: 0.2% CO, 0.2% O_2, He balance; CO: 0.2% CO, He balance.

intensity at 313–373 K was B-CO > L-CO ≈ T-CO. The intensity of T-CO decreased and that of B-CO increased significantly compared with that seen during the introduction of CO. Another important point is that all these three peaks were shifted to higher wavenumber (about 20–60 cm^{-1}) during the $CO + O_2$ reaction compared with during the introduction of CO. According to the previous report, adsorbed oxygen atoms occupy the threefold hollow sites on the Pt(111) surface [64]. In the

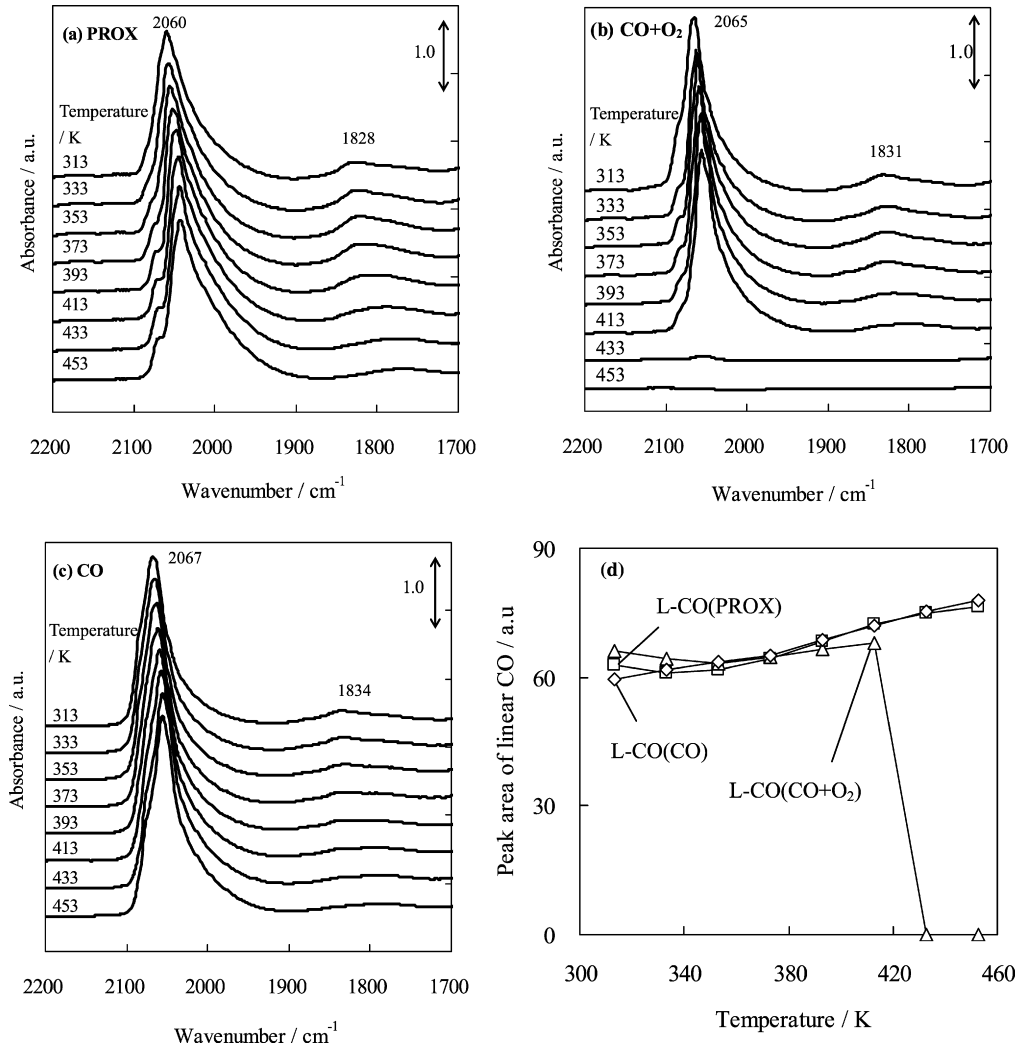

Fig. 8. Effect of temperature on IR spectra of Pt/Al_2O_3 catalyst during PROX (a), $CO + O_2$ (b) reactions and CO (c) introduction, (d) area of the linear CO peak as a function of temperature. (□) L-CO(PROX), (△) L-CO($CO + O_2$), (◇) L-CO(CO). Reaction conditions: PROX: 0.2% CO, 0.2% O_2, 75% H_2, He balance; $CO + O_2$: 0.2% CO, 0.2% O_2, He balance; CO: CO 0.2%, He balance.

coadsorption of oxygen and CO atoms, oxygen atoms are adsorbed on the threefold site and CO atoms are adsorbed mainly on the on-top site over Pt(111), Pd(111), and Rh(111) [64,65]. The coadsorption significantly affects the site of CO adsorption, suggesting that the CO adsorption site can be shifted to a site with lower coordination number. This can explain the change in adsorption site during the $CO + O_2$ reaction. In addition, the peak position of adsorbed CO was shifted to a higher wavenumber by the coordination of oxygen atoms [65]. From the comparison of the $CO + O_2$ reaction and the introduction of CO, the peak shift and the ratio change in the CO adsorption sites suggest that coadsorption of CO and oxygen occurred during the $CO + O_2$ reaction. In addition, the increased absorbance at around 1700 cm^{-1} may be due to adsorbed carbonate species originating from CO_2 produced by CO oxidation. Furthermore, in the case of $CO + O_2$, the peaks disappeared suddenly above 393 K (Fig. 7b). This represents the increased oxygen coverage and decreased CO coverage at higher reaction temperatures, which is expected based on the kinetics of CO oxidation with O_2 [66,67].

Figs. 7a and 7b show the behavior during this PROX reaction. At 313 K, the spectrum of PROX was similar to that of $CO + O_2$, with the order B-CO > L-CO ≈ T-CO. However, the shift of B-CO and T-CO was smaller in PROX than in $CO + O_2$. Note that the total peak area (L-CO + B-CO + T-CO; Fig. 7d) of PROX decreased slightly with increasing reaction temperature, and at 313–373 K, the decrease in PROX was more significant than that in $CO + O_2$. As shown in Fig. 7c, CO can be adsorbed on $K–Pt/Al_2O_3$ (10) when CO is present in the gas phase. This result suggests the presence of another adsorbed species with considerable coverage during the PROX reaction. Considering that the peak shift of PROX is smaller than that of $CO + O_2$, the adsorbed species can have less ability to accept electrons from Pt than oxygen atoms. It is expected that adsorbed species can be formed in the simultaneous presence of H_2 and O_2, and that candidates of the species are H_2O_2 and OOH. However, considering that Pt is usually unsuitable for the production of H_2O_2 from H_2 and O_2, these species are unlikely. Another plausible candidate is hydroxide species (OH). The OH group may be observed in FTIR spectra in higher wavenumber regions; how-

ever, such observation is difficult, because the peaks due to H_2O (a byproduct of the PROX reaction) overlap, and thus we do not yet have direct evidence of the OH group on Pt. The species and the reaction mechanism are discussed in more detail later.

Fig. 8 shows the temperature dependence of IR spectra of Pt/Al_2O_3 [773] during the PROX and $CO + O_2$ reactions and the introduction of CO. For Pt/Al_2O_3 [773], the spectra under these three conditions seemed to be similar below 433 K. This means that the coverage of adsorbed CO was close to the saturation level, and the coverage of coadsorbed species was rather low. The very small differences in the peak positions support this interpretation. At temperatures above 443 K in the $CO + O_2$ reaction, the peaks disappeared, as they did for $K–Pt/Al_2O_3$ (10), although the temperature on Pt/Al_2O_3 [773] was much higher than that on $K–Pt/Al_2O_3$ (10). This can be explained by the stronger interaction of CO with Pt/Al_2O_3 [773], as shown in Fig. 6.

3.4. Promoting effect of potassium on preferential CO oxidation over Pt/Al_2O_3

The addition of potassium weakened the interaction of Pt and CO, possibly due to the greater electron deficiency of the Pt species. This can contribute to high activity at lower reaction temperatures. Another important finding is that the adsorption site of CO was changed drastically. On $K–Pt/Al_2O_3$ (10), bridge and three-fold hollow CO species were clearly observed. The reason for the adsorption site change is not clear at present, but it may be related to the change in the electronic state of Pt modified by potassium. Based on the results of in situ FTIR observation, the coverage of CO on $K–Pt/Al_2O_3$ (10) during the PROX reaction was decreased, suggesting the presence of another coadsorbed species than oxygen atom. This species can promote CO oxidation. One possible candidate is the OH group, which can be formed by adsorbed hydrogen and oxygen atoms. It has been reported that the OH group promoted CO oxidation on Pt(111) [63,68], as described below:

$$H_{ad} + O_{ad} \rightarrow OH_{ad} \quad (1)$$

and

$$CO_{ad} + OH_{ad} \rightarrow CO_{2g} + H_{ad}. \quad (2)$$

These reaction formulas correspond to the reaction route via OH species as an autocatalytic mechanism [68]. In fact, the presence of H_2 enhanced the CO oxidation activity on Pt/Al_2O_3 at reaction temperatures below 420 K (Fig. 1b); however, the effect was as significant as that on $K–Pt/Al_2O_3$ (10) (Fig. 1a). This difference in the promoting effect of H_2 may be due to the difference in coverage of the OH species. Potassium plays a very important role in the enhancement of OH coverage, for example, by a Coulomb interaction between OH^- and K^+. In addition, judging from the low activity of the water–gas shift reaction, this active OH cannot be formed from H_2O in the gas phase.

4. Conclusion

The addition of potassium to Pt/Al_2O_3 significantly enhanced the activity of preferential CO oxidation in an H_2-rich stream. In particular, the presence of H_2 significantly promoted CO oxidation. According to the catalyst characterization by TEM and EXAFS, $K–Pt/Al_2O_3$ (10) had ca. 2-nm-diameter metal particles. Pt L_3-edge white line analysis revealed that Pt metal particles on $K–Pt/Al_2O_3$ were electron-deficient compared with those on the Pt/Al_2O_3 with similar metal particle sizes. FTIR observation of CO-TPD demonstrated much weaker CO adsorption on $K–Pt/Al_2O_3$ than on Pt/Al_2O_3, possibly related to the electron deficiency of $K–Pt/Al_2O_3$. The FTIR spectra suggest that CO was adsorbed on the bridge and three-fold hollow sites as well as on the on-top site on $K–Pt/Al_2O_3$. This behavior differed from that on Pt/Al_2O_3. In situ FTIR observations under the PROX conditions on $K–Pt/Al_2O_3$ at the low temperatures at which the PROX reaction proceeds indicated less CO adsorption compared with that in the $CO + O_2$ reaction and the introduction of CO. This suggests that the adsorbed species originating from H_2 and O_2 (e.g., the OH species) could be present on the surface and could promote CO oxidation.

References

[1] R. Farrauto, S. Hwang, L. Shore, W. Ruettinger, J. Lampert, T. Giroux, Y. Liu, O. Ilinich, Annu. Rev. Mater. Res. 33 (2003) 1.
[2] B. Rohland, V. Plzak, J. Power Source 84 (1999) 183.
[3] J. Divisek, H.-F. Oetjen, V. Peinecke, V.M. Schmidt, U. Stimming, Electrochim. Acta 43 (1998) 3811.
[4] C. Song, Catal. Today 77 (2002) 17.
[5] D.L. Trimm, Appl. Catal. A 296 (2005) 1.
[6] C. Pedrero, T. Waku, E. Iglesia, J. Catal. 233 (2005) 242.
[7] Y. Minemura, S. Ito, T. Miyao, S. Naito, K. Tomishige, K. Kunimori, Chem. Commun. (2005) 1429.
[8] Y. Minemura, M. Kuriyama, S. Ito, K. Tomishige, K. Kunimori, Catal. Commun. 7 (2006) 623.
[9] A. Manasilp, E. Gulari, Appl. Catal. B 37 (2002) 17.
[10] H. Igarashi, H. Uchida, M. Suzuki, Y. Sasaki, M. Watanabe, Appl. Catal. A 159 (1997) 159.
[11] I.H. Son, A.M. Lane, Catal. Lett. 76 (2001) 151.
[12] X. Liu, O. Korotkikh, R. Farrauto, Appl. Catal. A 226 (2002) 293.
[13] A. Sirijaruphan, J.G. Goodwin Jr., R.W. Rice, J. Catal. 221 (2004) 288.
[14] M.J. Kahlich, H.A. Gasteiger, R.J. Behm, J. Catal. 171 (1997) 93.
[15] S.H. Oh, R.M. Sinkevitch, J. Catal. 142 (1993) 254.
[16] O. Korotkikh, R. Farrauto, Catal. Today 62 (2000) 249.
[17] A. Fukuoka, M. Ichikawa, Top. Catal. 40 (2006) 103.
[18] M. Kotobuki, A. Watanabe, H. Uchida, H. Yamashita, M. Watanabe, J. Catal. 236 (2005) 262.
[19] M. Kotobuki, A. Watanabe, H. Uchida, H. Yamashita, M. Watanabe, Appl. Catal. A 307 (2006) 275.
[20] A. Sirijaruphan, J.G. Goodwin Jr., R.W. Rice, J. Catal. 224 (2004) 304.
[21] M.M. Schubert, M.J. Kahlich, G. Feldmeyer, M. Huttner, S. Hackenberg, H.A. Gasteiger, R.J. Behm, Phys. Chem. Chem. Phys. 3 (2001) 1123.
[22] C. Kwak, T.J. Park, D.J. Suh, Appl. Catal. A 278 (2005) 186.
[23] E. Simsek, S. Ozkara, A.E. Aksoylu, Z.I. Onsan, Appl. Catal. A 316 (2006) 169.
[24] M. Shou, K. Tanaka, Catal. Lett. 111 (2006) 115.
[25] S.H. Cho, J.S. Park, S.H. Choi, S.H. Kim, J. Power Sources 156 (2006) 260.
[26] J.L. Ayastuy, M.P. Gonzalez-Marcos, A. Gil-Rodriguez, J.R. Gonzalez-Velasco, M.A. Gutierrez-Ortiz, Catal. Today 116 (2006) 391.

[27] J.L. Ayastuy, M.P. Gonzalez-Marcos, J.R. Gonzalez-Velasco, M.A. Gutierrez-Ortiz, Appl. Catal. B 70 (2007) 532.
[28] J.L. Ayastuy, A. Gil-Rodriguez, M.P. Gonzalez-Marcos, M.A. Gutierrez-Ortiz, Int. J. Hydrogen Energy 31 (2006) 2231.
[29] G. Uysal, A.N. Akin, Z.I. Onsan, R. Yildirim, Catal. Lett. 108 (2006) 193.
[30] I.H. Son, J. Power Sources 159 (2006) 1266.
[31] S. Monyanon, S. Pongstabodee, A. Luengnaruemitchai, J. Power Sources 163 (2006) 547.
[32] E.Y. Ko, E.D. Park, K.W. Seo, H.C. Lee, D. Lee, S. Kim, Catal. Today 116 (2006) 377.
[33] B. Atalik, D. Uner, J. Catal. 241 (2006) 268.
[34] N. Iwasa, S. Arai, M. Arai, Catal. Commun. 7 (2006) 839.
[35] Y.F. Han, M.J. Kahlich, M. Kinne, R.J. Behm, Phys. Chem. Chem. Phys. 4 (2002) 389.
[36] H. Tanaka, S. Ito, S. Kameoka, K. Tomishige, K. Kunimori, Catal. Commun. 4 (2003) 1.
[37] H. Tanaka, S. Ito, S. Kameoka, K. Tomishige, K. Kunimori, Appl. Catal. A 250 (2003) 255.
[38] S. Ito, H. Tanaka, Y. Minemura, S. Kameoka, K. Tomishige, K. Kunimori, Appl. Catal. A 273 (2004) 295.
[39] S. Ito, T. Fujimori, K. Nagashima, K. Yuzaki, K. Kunimori, Catal. Today 57 (2000) 247.
[40] M.M. Schubert, V. Plzak, J. Garche, R.J. Behm, Catal. Today 76 (2001) 143.
[41] B. Schumacher, Y. Denkwitz, V. Plzak, M. Kinne, R.J. Behm, J. Catal. 224 (2004) 449.
[42] R.M. Torres Sanchez, A. Ueda, K. Tanaka, M. Haruta, J. Catal. 168 (1997) 125.
[43] F. Arena, P. Famulari, G. Trunfio, G. Borura, F. Frusteri, L. Spadaro, Appl. Catal. B 66 (2006) 81.
[44] M. Shou, H. Takekawa, D.Y. Ju, T. Hagiwara, D.L. Lu, K. Tanaka, Catal. Lett. 108 (2006) 119.
[45] M. Azar, V. Caps, F. Morfin, J. Rousset, A. Piednoir, J. Bertolini, L. Piccolo, J. Catal. 239 (2006) 307.
[46] C. Rossignol, S. Arrii, F. Morfin, L. Piccolo, V. Caps, J. Rousset, J. Catal. 239 (2006) 307.
[47] Y. Tanaka, T. Utaka, R. Kikuchi, K. Sasaki, K. Eguchi, Appl. Catal. A 238 (2003) 11.
[48] J. Papavasiliou, G. Avgouropoulos, T. Ioannides, Appl. Catal. B 66 (2006) 167.
[49] Y. Liu, Q. Fu, M.F. Stephanopoulos, Catal. Today 93–95 (2004) 241.
[50] J.W. Park, J.H. Jeong, W.L. Yoon, C.S. Kim, D.K. Lee, Y. K Park, Y.W. Rhee, Int. J. Hydrogen Energy 30 (2005) 209.
[51] S. Derrouiche, P. Gravejat, B. Bassou, D. Bianchi, Appl. Surf. Sci. 253 (2007) 5894.
[52] Y. Chen, K. Tomishige, K. Yokoyama, K. Fujimoto, Appl. Catal. A Gen. 165 (1997) 335.
[53] J.W. Cook, D.E. Sayers, J. Appl. Phys. 52 (1981) 5024.
[54] K. Okumura, J. Amano, N. Yasunobu, M. Niwa, J. Phys. Chem. B 104 (2000) 1050.
[55] K. Okumura, S. Matsumoto, N. Nishiaki, M. Niwa, Appl. Catal. B 40 (2003) 151.
[56] T. Kubota, K. Asakura, N. Ichikuni, Y. Iwasawa, Chem. Phys. Lett. 256 (1996) 445.
[57] T. Kubota, K. Asakura, Y. Iwasawa, Catal. Lett. 46 (1997) 141.
[58] A.N. Mansour, J.W. Cook, D.E. Sayers Jr., J. Phys. Chem. 88 (1984) 2330.
[59] J.A. Horsely, J. Chem. Phys. 76 (1982) 1451.
[60] H. Yoshida, Y. Yazawa, T. Hattori, Catal. Today 87 (2003) 19.
[61] L.F. Liotta, G.A. Martin, G. Deganello, J. Catal. 164 (1996) 322.
[62] N. Pavlenko, P.P. Kostrobij, Y. Suchorski, R. Imbihl, Surf. Sci. 489 (2001) 29.
[63] I.N. Yakovkin, V.I. Chernyi, A.G. Naumovets, Surf. Sci. 442 (1999) 81.
[64] K.L. Kostov, P. Jakob, D. Menzel, Surf. Sci. 377 (1997) 802.
[65] J. Libuda, H.-J. Freund, Surf. Sci. Rep. 57 (2005) 157.
[66] K. Nakao, S. Ito, K. Tomishige, K. Kunimori, J. Phys. Chem. B 109 (2005) 24002.
[67] T. Engel, G. Ertl, Adv. Catal. 28 (1979) 1.
[68] J. Bergeld, B. Kasemo, D.V. Chakarov, Surf. Sci. 495 (2001) L815.